ELSEVIER

Dynamics of Atmospheres and Oceans 27 (1997) 715–743

dynamics of atmospheres and oceans

Vertical vorticity development owing to down-sliding at slantwise isentropic surface

Guo-Xiong Wu [a,*], Huan-Zhu Liu [b]

[a] *State Key Laboratory of Atmospheric Sciences and Geophysicical Fluid Dynamics (LASG), Institute of Atmospheric Physics, Chinese Academy of Sciences, Beijing 100080, People's Republic of China*

[b] *National Meteorology Centre, China Meteorology Administration, Beijing 100086, People's Republic of China*

Received 12 January 1996; revised 1 October 1996; accepted 16 October 1996

Abstract

Based upon the conservation of Ertel potential vorticity and moist potential vorticity, a 'parcel dynamic' approach is used to investigate the development of vertical vorticity of a parcel which is sliding down a slantwise isentropic surface. An accurate form of the tendency equation of vertical vorticity is deduced to interpret such slantwise vorticity development (SVD). In addition to those dynamic terms in the traditional vertical vorticity equation, the newly developed accurate form includes several thermal terms associated with the changes in stability, vertical wind shear and baroclinity. It is proved that the combinative impacts of these thermal terms on the development of vertical vorticity can be expressed by a succinct theory of SVD. According to this theory, when the horizontal component of potential vorticity and stability possess opposite signs, and the slantwise isentropic surfaces are very steep, the vorticity development of the down-sliding flow at such isentropes can be dramatic. It is also shown that in a convectively unstable and saturated atmosphere, such vorticity development must be accompanied by the development of a low-level jet. Study of a torrential rain process shows that moist potential vorticity analysis is a powerful tool in the study of torrential rain occurrence. Results from the present study are in agreement with the contentions of earlier workers that moist symmetric instability is the cause of some heavy rainbands. © 1997 Elsevier Science B.V.

1. Introduction

In a frictionless and adiabatic dry atmosphere, the Ertel potential vorticity P_E is conserved (Ertel, 1942). The application of the Ertel potential vorticity in the diagnosis of atmospheric motion has been summarised by Hoskins et al. (1985). The concept of

* Corresponding author.

PII S0377-0265(97)00040-7

isentropic potential vorticity (IPV) was also introduced. Generally speaking, IPV is indicative of some aspects of the movement and development of weather systems in middle and high latitudes. However, in the lower troposphere, especially in low latitudes, IPV becomes very weak. Besides, IPV does not include the effects of moisture. Thus the application of IPV analysis is not so good in the lower troposphere, low-latitude regions and in precipitation cases.

To consider the impacts of moisture, Bennetts and Hoskins (1979) used an equation set with Boussinesq approximation and deduced an equation for the variation of the so-called 'wet-bulb potential vorticity'. Based on the accurate primitive equation set, a similar variation equation for moist potential vorticity (MPV) was also obtained by Wu et al. (1995). Their research showed that in a frictionless and adiabatic saturated atmosphere, MPV is conserved.

Another issue which has attracted much attention is the impacts of such conservation properties on atmospheric motion. Based on Lagrangian parcel dynamics, Emanuel (1984) developed a simple model to describe the slantwise ascent of a two-dimensional horizontal air tube, and found that moist symmetric instability is the cause of some mesoscale rainbands, in agreement with the findings of Bennetts and Hoskins (1979). In this study, we use the 'parcel dynamics' approach to investigate how a slowly descending parcel on a slantwise isentropic surface changes its vertical vorticity under the constraint of constant potential vorticity. In a dry atmosphere, the vorticity development of a parcel owing to its down-sliding along a slantwise isentropic surfaces, which is termed slantwise vorticity development (SVD), is discussed in Section 2. An accurate form of vertical vorticity tendency equation is developed in Section 3 to interpret SVD, and the importance of geostrophy in the issue is discussed in Section 4. In Section 5, a numerical experiment based upon a θ-coordinate is designed to verify how the development of an α-scale vortex can be explained by SVD. The SVD in a saturated atmosphere is studied in Section 6. In Section 7, the connection between the frequently observed low-level jet associated with torrential rain and SVD in a convectively unstable atmosphere is studied. In Section 8 the theory developed in the preceding sections is employed to diagnose a torrential rain process on 11–15 June 1991 during a monsoonal frontogenesis. A discussion and some conclusions are presented in Section 9.

2. Slantwise vorticity development in a dry atmosphere

In dry or unsaturated atmosphere which is frictionless and adiabatic, the conservation of Ertel potential vorticity P_E can be expressed as

$$\frac{DP_E}{Dt} = 0 \tag{1}$$

or,

$$P_E = \alpha \boldsymbol{\zeta}_a \cdot \nabla\theta = \text{constant} \tag{2}$$

where $\boldsymbol{\zeta}_a$ is absolute vorticity, θ is potential temperature, α is specific volume, and ∇ is three-dimensional Hamiltonian operator. We let $\boldsymbol{\Omega}$ denote the angular velocity of the Earth, and $\boldsymbol{V}$ the three-dimensional (3-D) wind vector; then

$$\boldsymbol{\zeta}_a = \nabla \times \boldsymbol{V} + 2\boldsymbol{\Omega} \tag{3}$$

If the slope of a θ surface with respect to the horizon is negligible, one can use θ as vertical coordinate. The advantage of this comes from the fact that along the isentropic surface, $\nabla_\theta \theta$ vanishes. Therefore, the conservation of P_E takes a simple form,

$$P_E = \alpha \zeta_\theta \frac{\partial \theta}{\partial z} \approx \text{constant} \tag{4}$$

and is sometimes referred to as isentropic potential vorticity (IPV). It should be noted that Eq. (4) is accurate only when the θ surfaces lies horizontally. When the θ surface declines, the accurate form of conservation should be rewritten as

$$P_E = \alpha \zeta_\theta |\nabla \theta| = \text{constant} \tag{5}$$

where ζ_θ is the projection of $\boldsymbol{\zeta}_a$ on $\nabla\theta$. Based on Eq. (5) we first investigate some fundamental relations which will be used later.

2.1. Box law

Let us suppose θ surfaces are planes and $|\nabla\theta|$ is constant. We imagine that a box has θ_1 and θ_2 as its bottom surface and top surface, respectively, and $\Delta\theta = |\alpha\zeta_\theta|$ as its thickness, and that the origin of the vector of $\alpha\boldsymbol{\zeta}_a$ of a parcel A is at the location of the parcel. Then the conservation of P_E as expressed by Eq. (5) together with the conservation of potential temperature can be presented in Fig. 1(a) and stated by the following 'box law':

> No matter how a parcel moves and spins on one side of the box θ_1, the head point of its specific absolute vorticity $\alpha\boldsymbol{\zeta}_a$ must be always on the opposite side of the box θ_2 $(= \theta_1 + \Delta\theta)$.

2.2. Circumscribed plane law

Let us suppose θ surfaces are spheres (Fig. 1(b)) and $|\nabla\theta|$ is constant. We imagine that the inner sphere θ_1 and the outer sphere θ_2 are separated by $\Delta\theta = |\alpha\zeta_\theta|$, and that the origin of the vector $\alpha\boldsymbol{\zeta}_a$ of a parcel A moving at sphere θ_1 is at the location of the parcel. We let B at sphere θ_2 be in line with the radius OA, and plane P the circumscribed plane of sphere θ_2 at B. Then the conservation of P_E as expressed by Eq. (5) together with the conservation of potential temperature can be presented in Fig. 1(b) and stated by the following 'circumscribed plane law':

> No matter how a parcel moves and spins at the sphere θ_1, the head point of its specific absolute vorticity $\alpha\boldsymbol{\zeta}_a$ must be always at the circumscribed plane P of θ_2 $(= \theta_1 + \Delta\theta)$ at B.

As the projection on $\nabla\theta$ of a $(\alpha\boldsymbol{\zeta}_a)$ which has its head point at the plane P equals $\overline{AB} = \alpha\zeta_\theta$, then under the constraint of conservation of Ertel potential vorticity P_E (Eq. (5)), the above 'circumscribed plane law' becomes self-explanatory. A very important point implied by the 'circumscribed plane law' is that a change in one component of $\alpha\boldsymbol{\zeta}_a$ will cause changes in its other components. In other words, once the horizontal component of a $(\alpha\boldsymbol{\zeta}_a)$ is known, its vertical component can be uniquely determined

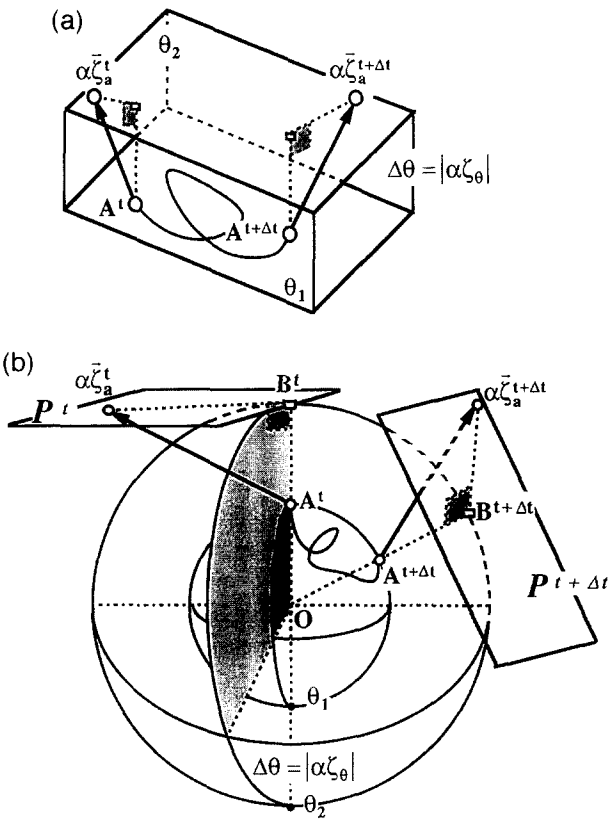

Fig. 1. (a) 'Box Law': for plane θ surfaces, no matter how a parcel moves and spins at one side of the box θ_1, the head point of its specific absolute vorticity ($\alpha\zeta_a$) must be always on the opposite side of the box θ_2 ($=\theta_1+\Delta\theta$). (b) 'Circumscribed Plane Law': for curved θ surfaces, no matter how a parcel moves and spins at the surface θ_1, the head point of its specific absolute vorticity ($\alpha\zeta_a$) must be always at the circumscribed plane P of θ_2 ($=\theta_1+\Delta\theta$) at B. (see text for details.)

from the circumscribed plane. This provides the basis for the theory of vertical vorticity development to be explored below. In developing both the 'box law' and 'circumscribed plane law', constant $|\nabla\theta|$ has been assumed. As we will discuss below, this assumption does not affect our following discussion. Because under the constrain of P_E conservation, Eq. (5), for the variation of vertical vorticity, a change in $|\nabla\theta|$ is always compensated for by a corresponding change in $\alpha\zeta_a$.

2.3. Slantwise vorticity development (SVD)

If z-coordinate is adopted, then

$$P_E = \alpha\zeta_z\frac{\partial\theta}{\partial z} + \alpha\zeta_s\frac{\partial\theta}{\partial s} = \text{constant} \tag{6}$$

where $\partial\theta/\partial s$ is the horizontal gradient of θ with the horizontal unit vector s perpendicular to isentropes, ζ_z is the vertical component of $\boldsymbol{\zeta}_a$, and $\zeta_s = \partial V_m/\partial z$ is the projection

on s of ζ_a, which is determined by the vertical shear of the wind V_m, which is perpendicular to, and positive on the right-hand side of, s. From Eq. (5) and Eq. (6) we obtain

$$P_E = \alpha\zeta_z\frac{\partial\theta}{\partial z} + \alpha\zeta_s\frac{\partial\theta}{\partial s} = \alpha\zeta_\theta\frac{\partial\theta}{\partial n} = \text{constant}$$

Here, we have already replaced $\nabla\theta$ by $(\partial\theta/\partial n)\boldsymbol{n}$, or $\theta_n\boldsymbol{n}$, and the unit vector $\boldsymbol{n}$ satisfies $\boldsymbol{n}\cdot\boldsymbol{k} > 0$, in which $\boldsymbol{k}$ is a geometrically upward unit vector. On denoting the absolute vorticity per unit mass as $\xi_a = \alpha\zeta_a$, and $\xi_n = \alpha\zeta_\theta$, the above relation can be written as

$$P_E = \xi_z\theta_z + \xi_s\theta_s = \xi_n\theta_n = \text{constant} \tag{7}$$

From this, we have

$$\xi_z = (\xi_n\theta_n - \xi_s\theta_s)/\theta_z \quad (\theta_z \neq 0) \tag{8}$$

This means that the change of vertical vorticity can result from the changes in static stability θ_z, vertical wind shear ξ_s, or baroclinity θ_s. It is important to note that the change in θ_n does not affect the vertical vorticity. This is because under the constraint of conservation of P_E (see Eq. (7)), the change in θ_n should always be compensated for by the change in ξ_n so that the product $(\xi_n\theta_n)$ appearing in Eq. (8) remains unchanged.

To understand how the slope of the isentropic surface affects the change of vertical vorticity, in Fig. 2 we assume that the parallel isentropes are horizontal to the right of

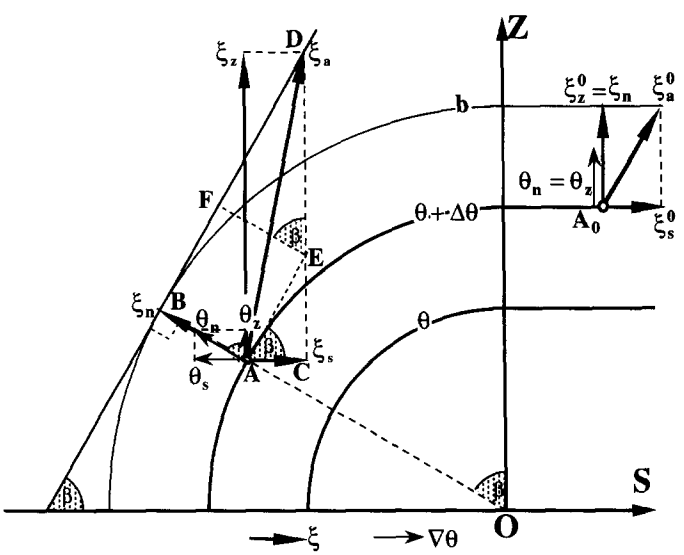

Fig. 2. Schematic diagram showing the development of vertical vorticity in a dry atmosphere owing to the slantwise sloping of the isentropic surface. When a parcel A_0 is initially on the horizontal part of a θ surface, $P_E = \xi_n^0\theta_n$ is independent of ξ_s. When it slides down the θ surface at an angle $\beta(<0)$ to A, then $\xi_z = (\xi_n/\cos\beta) - \xi_s\tan\beta$ can be expressed by $\xi_z = \overline{CD} = \overline{DE} + \overline{EC}$, or $\xi_z = \dfrac{\overline{AB}}{\cos\beta} + \overline{AC}|\tan\beta|$. Now, the increase in ξ_s or in $|\beta|$ may result in the development of ξ_z.

the z-coordinate, but are bent as circles to its left. For simplicity, as in deducing the box law and the circumscribed plane law, we further assume that the gradient of isentropes θ_n is constant. We let 'b' be such a circle, which is coaxial with the θ surface and keeps from it at a constant distance $\overline{AB} = |\xi_n|$. Then, according to the circumscribed plane law, for an air parcel originally at point A_0, and moving at the isentrope $\theta + \Delta\theta$ by sliding down an angle β (β is positive when one side deviates from z towards S) to point A, the head point D of $\boldsymbol{\xi}_a$ of the parcel A should be located in a plane DB which is a tangent to circle b at point B, as shown in Fig. 2. The central angle $\beta = \angle AOZ$ indicates the degree of deviation of the parcel A from the z-coordinate. β is positive when A is in the ZOS quadrant, and vice versa. Because, according to the figure,

$$\tan\beta = \theta_s/\theta_z \quad (-\pi/2 < \beta < \pi/2) \tag{9}$$

and as $\boldsymbol{n}\cdot\boldsymbol{k} > 0$, then

$$\cos\beta = \theta_z/\theta_n > 0$$

According to Eq. (3), in the northern hemisphere in the case of cyclogenesis, $\xi_n > 0$, Eq. (8) can then be expressed as

$$\xi_z = \frac{\xi_n}{\cos\beta} - \xi_s\tan\beta, \quad |\beta| \neq \pi/2 \tag{10}$$

In general, for ξ_s, θ_s and θ_z, each can be either positive or negative. However, it is important that in Eq. (7), if the following condition is satisfied:

$$C_D = \xi_s\theta_s/\theta_z < 0 \tag{11}$$

then Eq. (8) or Eq. (10) can be written as

$$\xi_z = \frac{\xi_n}{\cos\beta} + |\xi_s\tan\beta|, \quad |\beta| \neq \pi/2 \tag{12}$$

Geometrically, the relationship Eq. (12) can be interpreted by using Fig. 2 as

$$\xi_z = \overline{CD} = \overline{DE} + \overline{EC} = \frac{\overline{AB}}{\cos\beta} + \overline{AC}|\tan\beta| \tag{13}$$

where an overbar denotes the scalar length of the line segment. To satisfy Eq. (11), when plotting Fig. 2 we assumed that the vertical wind shear of the atmosphere is constant so that $\xi_s = \xi_s^0 > 0$. Otherwise, if ξ_s becomes negative, condition Eq. (11) will be violated and, from Fig. 2, ξ_z will decrease with increasing $|\beta|$. In our present case, when Eq. (11) is satisfied, Eq. (12) shows that ξ_z is an increasing function of $|\beta|$. This means that when an air parcel is sliding down the slope of a θ surface, its vertical vorticity will increase so long as condition Eq. (11) is satisfied. It also shows that ξ_z can be extremely large when the θ surface is steeply sloped. Because, in such circumstances, the development of vorticity is due to the down-sliding of the air parcel along a slantwise isentropic surface, it can be referred as down-sliding slantwise vorticity

development (SVD). On the other hand, if the isentropic surface is approximately horizontal, then

$$\xi_z \to \xi_n, \text{ if } \beta \to 0$$

Only to this extent is Eq. (4) applicable, and IPV becomes exactly conservative.

3. An accurate form of the vertical vorticity tendency equation and conditions for SVD

3.1. Vertical vorticity tendency equation

Upon applying material derivative to the both sides of Eq. (8), and using the continuity equation

$$\frac{D\alpha}{Dt} = \alpha \nabla \cdot V$$

an accurate form of tendency equation for the vertical vorticity component ξ_z can be obtained as

$$\frac{D\zeta_z}{Dt} + \beta v + (f + \zeta_z)\nabla \cdot V = -\frac{1}{\alpha(\theta_z)^2}\left[(P_E - \xi_s\theta_s)\frac{D\theta_z}{Dt} + \theta_z\xi_s\frac{D\theta_s}{Dt} + \theta_z\theta_s\frac{D\xi_s}{Dt}\right], \quad \theta_z \neq 0 \tag{14}$$

The right-hand side of the above equation indicates how the changes in static stability (θ_z), baroclinity (θ_s), and vertical wind shear (ξ_s) affect the development of vertical vorticity. If the right-hand side vanishes, then Eq. (14) becomes similar to the well-known traditional vertical vorticity tendency equation under frictionless as well as adiabatic constraints. It can be accurate if and only if the changes in static stability θ_z and in the horizontal component of P_E ($= \xi_s\theta_s$) are ignored. When isentropes lie horizontally, i.e. when $\theta_s \equiv 0$, Eq. (14) becomes

$$\frac{D}{Dt}\left[(f + \zeta_z)\frac{\partial\theta}{\partial z}\right] = \frac{D}{Dt}[\text{IPV}] = 0 \tag{14'}$$

This indicates that if and only if isentropes lie horizontally is IPV conserved and Eq. (4) takes an equal form. During cyclogenesis and the development of torrential rain or typhoon, the thermal structure of the atmosphere changes rapidly. In such circumstances, the traditional vertical vorticity equation becomes inaccurate, and the complete form of Eq. (14) should be considered.

For a statically stable atmosphere as shown in Fig. 2, θ_z is positive. When condition Eq. (11) is satisfied, $(P_E - \xi_s\theta_s)$ is positive as well. Also, when the parcel is sliding down the $\theta + \Delta\theta$ surface from A_0 to A, both $D\theta_z/Dt$ and $D\theta_s/Dt$ are negative. All these then contribute to the development of vertical vorticity. It should be noted that $(\theta_z)^2$ appears as a common denominator of the right-hand side terms. Therefore when an

air parcel slides down an isentrope which is steeply sloped, SVD can be dramatic, as was elucidated in Fig. 2.

3.2. Conditions for down-sliding SVD

Eq. (14) can be written in the following form:

$$\frac{1}{\alpha}\frac{\mathrm{D}\xi_z}{\mathrm{D}t} = \frac{\mathrm{D}\zeta_z}{\mathrm{D}t} + \beta v + (f+\zeta_z)\nabla\cdot\boldsymbol{V} = \frac{1}{\alpha}\frac{\mathrm{D}}{\mathrm{D}t}\left[\frac{P_{\mathrm{E}}}{\theta_z} - C_{\mathrm{D}}\right], \quad \theta_z \neq 0 \tag{15}$$

Then the SVD condition for the development of ξ_z or ζ_z is

$$C_{\mathrm{D}}(t+\Delta t) - C_{\mathrm{D}}(t) < P_{\mathrm{E}}\left[\frac{1}{\theta_z(t+\Delta t)} - \frac{1}{\theta_z(t)}\right], \quad \theta_z \neq 0 \tag{16}$$

Similarly, when the air parcel is moving downslope of the θ-surface by an angle $\Delta\beta$, then the condition for SVD is

$$C_{\mathrm{D}}(\beta+\Delta\beta) - C_{\mathrm{D}}(\beta) < P_{\mathrm{E}}\left[\frac{1}{\theta_z(\beta+\Delta\beta)} - \frac{1}{\theta_z(\beta)}\right], \quad \theta_z \neq 0 \tag{17}$$

Because only under condition Eq. (17) is $\mathrm{D}\xi_z/\mathrm{D}t > 0$, Eq. (17) is a necessary condition for SVD. For the case shown in Fig. 2, the right-hand side of Eq. (17) is positive. Because C_{D} at A_0 is zero, as the isentrope there is horizontal, a negative C_{D} at A thus satisfies Eq. (17) automatically, and condition Eq. (11) is therefore a sufficient condition for SVD.

4. Geostrophy and slantwise vorticity development

For convenience, in this section we temporary adopt the p-coordinate for discussion. In this case,

$$P_{\mathrm{E}} = -g(f\boldsymbol{k} + \nabla_p \times \boldsymbol{V})\cdot\nabla_p\theta = \text{constant} \tag{18}$$

We define the vertical component of P_{E} as the first component, and the horizontal component as the second component, i.e.

$$\begin{cases} PV1 = -g\zeta_p\dfrac{\partial\theta}{\partial p}, \\ PV2 = -g\boldsymbol{k}\times\dfrac{\partial\boldsymbol{V}}{\partial p}\cdot\nabla_p\theta \end{cases} \tag{19}$$

where $\zeta_p = \mathrm{f} + (\partial v/\partial x - \partial u/\partial y)$. Then the conservation of P_{E} can be expressed as

$$P_{\mathrm{E}} = PV1 + PV2 = \alpha\zeta_\theta|\nabla\theta| = \text{constant} \tag{20}$$

and the condition Eq. (11) for down-sliding SVD becomes

$$PV2/\theta_p > 0 \tag{21}$$

This means that the horizontal component of P_E and static stability possess opposite signs. Supposing that the atmospheric motion satisfies the geostrophic relation

$$\boldsymbol{V} = f^{-1}\boldsymbol{k} \times \nabla_p \Phi$$

then

$$\frac{\partial \boldsymbol{V}}{\partial p} = f^{-1} R^* \boldsymbol{k} \times \nabla_p \theta$$

where

$$R^* = C_p^{-1} p^{-1} R\pi$$

and the Exner function

$$\pi = C_p \left(p p_0^{-1} \right)^{\kappa}$$

After some manipulation, we obtain

$$PV2 = -\frac{\alpha g}{f\theta_0} |\nabla_p \theta|^2 < 0 \tag{22}$$

where θ_0 is the potential temperature at the P_0 surface. According to Eq. (22), for a geostrophic atmosphere to satisfy Eq. (21), θ_p should be negative. This is to say that, in a statically stable atmosphere, SVD can occur under the geostrophic balance, whereas in a statically unstable atmosphere ($\theta_p > 0$), the condition Eq. (21) for down-sliding SVD cannot be satisfied under the geostrophic balance.

5. A numerical experiment

In the period from 11 to 15 July 1981 in Sichuan Province, Southwestern China, there occurred persistent heavy rainfall. At the centre of precipitation, the total rainfall was over 366 mm and concentrated from 12 to 14 July, causing the most severe damage during the past 40 years. It was so strong and so disastrous that its occurrence has attracted world-wide interest. Many researchers (e.g. Hovermale, 1984; Anthes and Heagerson, 1984; Chen and Dell'Osso, 1984; Zhou and Hu, 1984; Kuo et al., 1986) diagnosed and simulated the weather system associated with the development of the rainfall. The common conclusion was that the torrential rain was caused by the rapid development of an α-scale vortex in Southwestern China, usually called a 'southwest vortex' in the Chinese literature. A cyclonic circulation was first detected on the weather chart at 12:00 h, 11 July 1981, at the southeastern edge of the Tibetan Plateau, then moved to the Sichuan Basin on 12 July and developed as a SW vortex with the centre located at 104°E, 28°N. At the same time, on the northeastern flank of the Tibetan Plateau, there was a mid-latitude trough developing and moving eastwards. A situation

with a trough in the north and a vortex in the south, which favours the occurrence of torrential rain in the Sichuan area, occurred on 12 July along the eastern edge of the Plateau (Zhou and Hu, 1984).

Although the release of latent heat owing to condensation of water vapour is important for the development of a SW vortex, its formation is associated more with the mechanical forcing of the Tibetan Plateau (Wu and Chen, 1985). This makes it practical to use the model of Bleck (1984) to simulate the formation of the vortex. The model is adiabatic and uses the θ-surface as vertical coordinate. Its basic set of equations is composed of the following:the momentum equations

$$\left(\frac{\partial u}{\partial t}\right)_\theta + \boldsymbol{V}\cdot\nabla_\theta u - fv = -\left(\frac{\partial M}{\partial x}\right)_\theta + F_x$$

$$\left(\frac{\partial v}{\partial t}\right)_\theta + \boldsymbol{V}\cdot\nabla_\theta v - fu = -\left(\frac{\partial M}{\partial y}\right)_\theta + F_y$$

the continuity equation

$$\frac{\partial}{\partial t}\left(\frac{\partial p}{\partial \theta}\right) + \nabla_\theta\cdot\left(\boldsymbol{V}\frac{\partial p}{\partial \theta}\right) = 0$$

the thermodynamic equation

$$\frac{\mathrm{D}\theta}{\mathrm{D}t} = 0$$

and the hydrostatic equation

$$\frac{\partial M}{\partial \theta} = \pi$$

where F_x and F_y are the components of frictional force in the x- and y-directions, respectively, $M = \Phi + C_pT$ is the Montgomery function, and $\pi = C_p(p/p_0)^{R/C_p}$ is the Exner function. In the vertical the model atmosphere is divided into 13 layers ranging from 305 K to 365 K with an equal interval of 5 K. The horizontal grid size is 80 km. The domain of integration covers an area of 44×49 grid points. The length of time step for integration is 60 s. The lateral boundary conditions for each variable at each time step are obtained by using linear interpolation of observation data between its initial value and the value at the end of integration. The details of the model, particularly the treatment of the lower boundary, have been given by Bleck (1984).

Zhao et al. (1995) introduced the distribution of orography over China into the model, chose the meteorological fields at 00:00 h, 11 July 1981 as the initial state, then integrated the model for 60 h to simulate the formation of the SW vortex. The formation of the vortex was reasonably simulated during the first 24 h. Below, we will use the material extracted from this integration to study how the formation of the vortex and the development of the mid-latitude trough to its north can be interpreted in terms of the SVD theory developed above. Because over the Sichuan Basin and in the formation stages of the vortex, the elevation of the coordinate surface $\theta = 315$ K is near 750 hPa (see Fig. 4 and Fig. 5, below), just passing through the upper part of the generated

vortex, the distributions of various variables at this surface will be used for the following diagnosis.

In Fig. 3 are shown the distributions of the initial fields at $\theta = 315$ K and 00:00 h, 11 July 1981. A remarkable characteristic of the θ surface is that it was highly uplifted over the Plateau and sharply tilted downwards onto the surrounding areas with geometric height lower than 2 km (Fig. 3(a)). The highest altitude of the θ surface over the Plateau was at 493 hPa, whereas that over the Sichuan Basin and Gobi desert was at 817 hPa and 863 hPa, respectively. As the model is adiabatic, a parcel which is initially at this θ surface will be detained at the surface during its later travelling. As the θ surface is steeply tilted at the edge of the Plateau, a wind feather at the surface pointing from low pressure towards high pressure and crossing the edge will slide down the steeply slantwise θ surface, and is presented by a heave feather with an arrowhead. In the initial field, along the eastern edge of the Plateau $\xi_n = \alpha(f + \zeta_n)$ was positive (see Fig. 3(b)), as was θ_n. The air there was then symmetrically stable ($P_E > 0$). According to the distribution of θ, the horizontal gradient of isentropes s in this area was outward from the Plateau. Because the southerlies near the surface increased with height (Zhou and Hu, 1984), the vertical wind shear $\xi_s (= \partial V_m / \partial z)$ there possessed opposite sign to θ_s, and $C_D = \xi_s \theta_s / \theta_z$ was negative. Therefore the sufficient condition Eq. (11) for SVD was satisfied, and vertical vorticity development along the eastern edge of the Plateau should be anticipated. Fig. 3(b) shows the simultaneous distribution of vertical vorticity at the same surface. As the distributions of vertical vorticity at the adjacent θ surface (figures not shown) are similar to that of Fig. 3(b), interpolation of the vorticity field onto an intermediate pressure or z-coordinate surface will not change the general characteristics of the distribution. For simplicity, hereafter we will use the vorticity distribution at this θ surface as a perspective of the vertical vorticity distribution at a nearby pressure or z-coordinate surface.

In Fig. 3(b), two positive centres appeared, one over the northeastern flank of the Plateau with an intensity of $3.15 \times 10^{-5}\ s^{-1}$, the other over the southeastern flank with an intensity of $4.33 \times 10^{-5}\ s^{-1}$. The former was associated with the movement of the mid-latitude trough, and the latter, as we will see, was associated with a new-born cyclonic vortex. They appeared in the region where the wind vectors slide down the steeply tilted θ surface. In this figure, positive vorticity centres are also observed over eastern China and Bohai Bay, western Pacific, the Indochina Peninsula, and the Bay of Bengal. They were associated with specific weather systems. As these centres appeared in the regions where the θ surface was relatively flat, not relevant to our topic, we will not pay attention to their evolution and only confine ourselves to the development of the two centres along the eastern edge of the Plateau.

At 12 h later (Fig. 4), the pressure pattern at the 315 K surface was unchanged (Fig. 4(a)). However, the warm funnel over the Sichuan Basin stretched downwards from 817 hPa to 842 hPa. Compared with the initial field, the most striking change was the strengthening of the down-sliding wind vectors along the northeastern edge and over the southeastern flank of the Plateau. The down-sliding area expanded, the wind speed intensified, and the wind vector became more perpendicular to the isobars. The down-sliding over the southeastern flank was split into two branches; that in the west was near 98°E, and that in the east had already slid down onto the Sichuan Basin. In

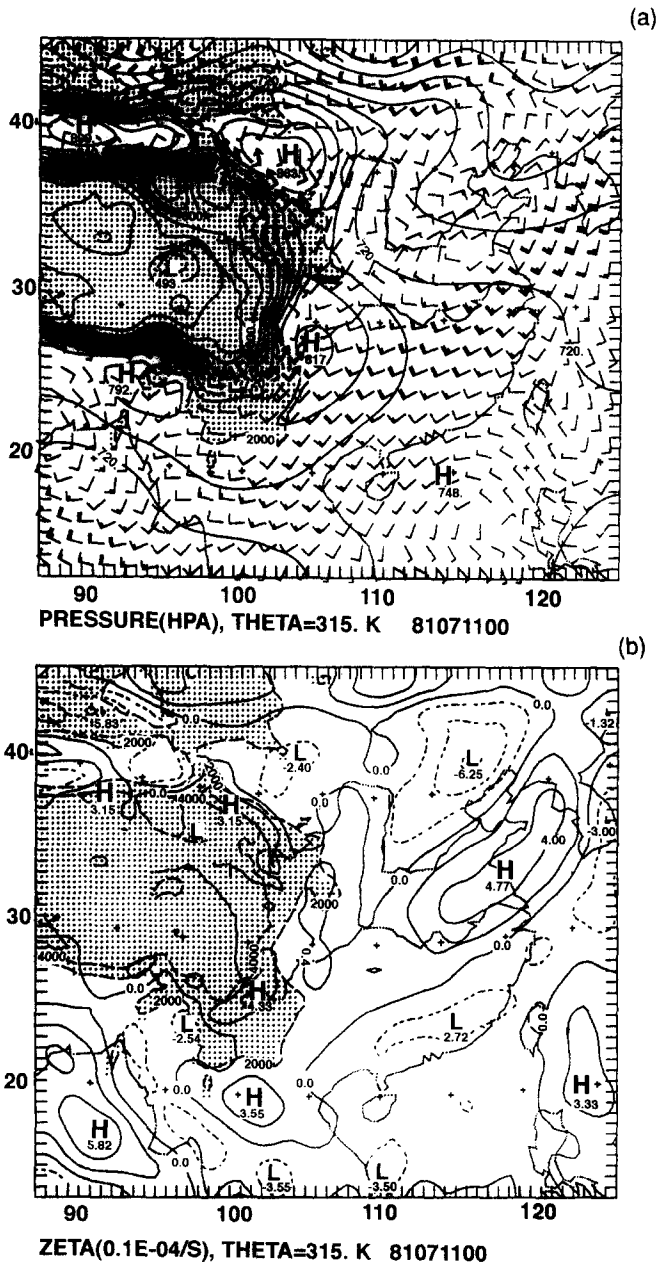

Fig. 3. The distributions at the $\theta = 315$ K surface and 00:00 h, 11 July 1981 of pressure contour (interval in 30 hPa) and wind vector (a), and of vertical vorticity (interval in $2.00 \times 10^{-5}\,s^{-1}$) (b). Each bar of the wind feather in (a) represents $4\,m\,s^{-1}$. The heavy feather with arrowhead denotes that the wind vector is down-sliding on the steeply tilted θ surface.

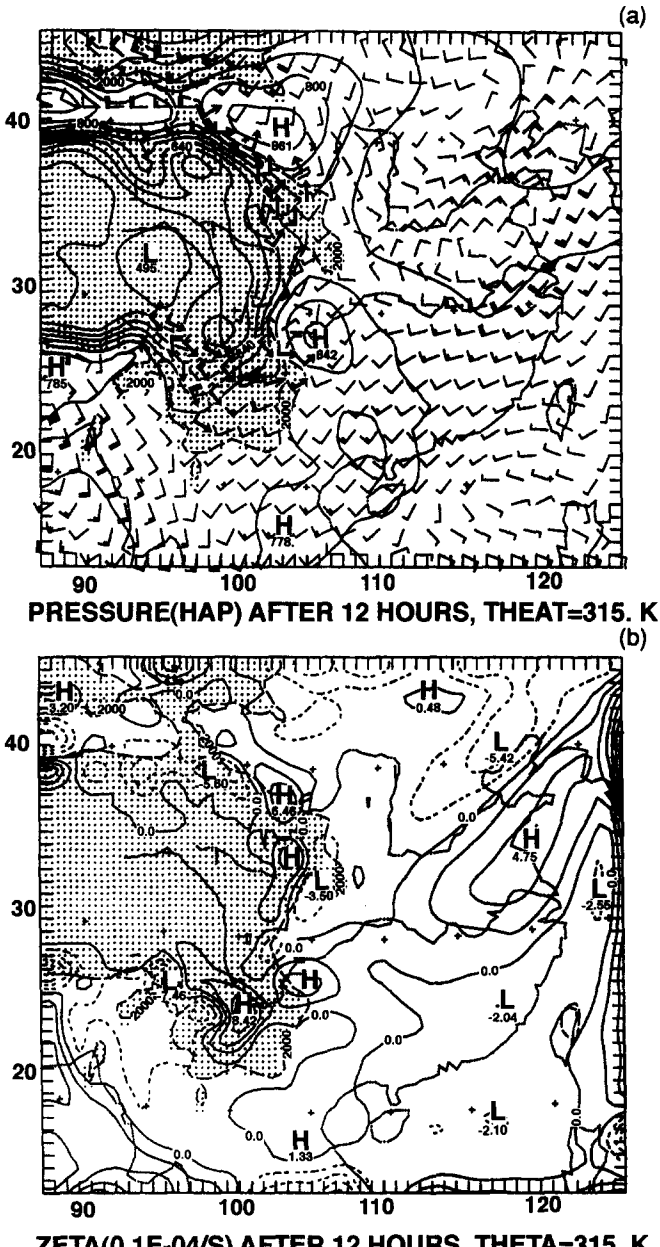

Fig. 4. The same as in Fig. 3 except that the modelled distributions are at 12:00h, 11 July 1981. The contour interval is 40hPa in (a), and $2.00 \times 10^{-5}\,s^{-1}$ in (b).

response to the rapid intensification of the down-sliding flow, the associated vertical vorticity developed dramatically during this period (Fig. 4(b)). The northern centre expanded and moved eastwards. Its intensity was $6.46 \times 10^{-5}\,s^{-1}$, more than double its

initial value. The southern centre developed even more vigorously. It was split into two systems. The intensity of the western centre was nearly doubled, reaching $8.42 \times 10^{-5}\ s^{-1}$. The eastern centre had an intensity of more than $4 \times 10^{-5}\ s^{-1}$, and started to

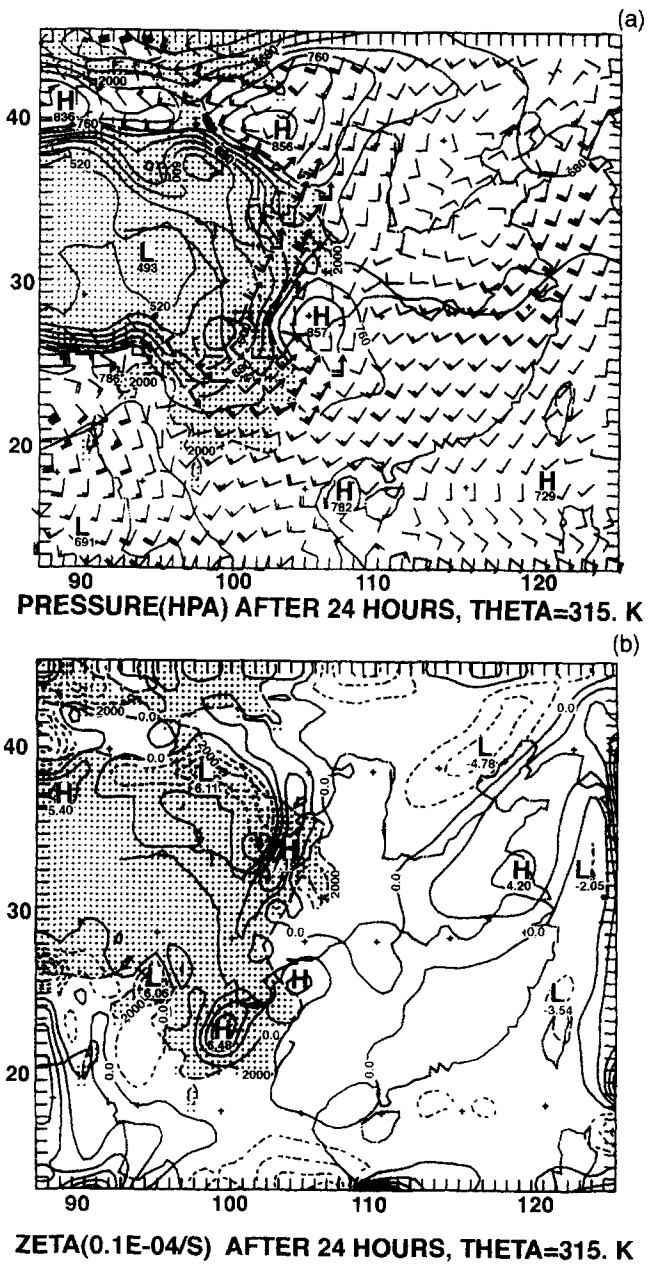

Fig. 5. The same as in Fig. 3 except that the modelled distributions are at 00:00 h, 12 July 1981. The contour interval is 40 hPa in (a) and $2.00 \times 10^{-5}\ s^{-1}$ in (b).

enter the Sichuan Basin. At that moment, the SW vortex had actually formed, although only a part of the centre appeared over the Basin.

By 00:00 h, 12 July, the pressure pattern around the Plateau at the 315 K surface was still similar (Fig. 5(a)). The warm funnel over the Sichuan Basin moved eastward slowly and stretched further downwards again, reaching 857 hPa. The down-sliding flow at the eastern edge of the Plateau also shifted eastwards, and intensified. The strengthened down-sliding flow in the north caused the further development of the mid-latitude trough (Fig. 5(b)). Its vertical vorticity was increased to $7.19 \times 10^{-5}\,s^{-1}$. In the south, the weakening of the down-sliding flow near 98°E caused the weakening of the western vorticity centre at 100°E. As to the eastern centre, although to its south the slope of the 315 K surface was less steep, the down-sliding southwesterlies there became stronger, so that the intensity of the SW vortex was almost unchanged. Furthermore, the eastward movement of the warm funnel and the intensification of the associated down-sliding flow caused the SW vortex to move eastward as well. The whole centre of the vortex was over the Sichuan Basin. Up to this stage, a complete SW vortex was observed there. Its location coincided very well with that of the observed new-born vortex (104°E, 28°N). The results presented in this section thus demonstrate that Bleck's adiabatic model can simulate well the formation of the SW vortex, and the intensification of the mid-latitude trough and the formation of the SW vortex can be interpreted by using the SVD theory.

One may suspect that the aforementioned vorticity development could result from the vertical stretching of the air column when sliding down the slope of a mountainside, as is usually suggested. In this aspect we may enlist the help of Eq. (14) and the continuity equation. We then have

$$\frac{D\zeta_z}{Dt} \alpha -(f+\zeta_z)\frac{1}{\alpha}\frac{D\alpha}{Dt} = \frac{(f+\zeta_z)}{1-\kappa}\frac{\omega}{p}$$

Taking $p = 700\,hPa$, $\omega = 1 \times 10^{-3}\,hPa\,s^{-1}$, $\varphi = 30°N$, and $\Delta t = 0.5\,day$, then the increase of vorticity of a down-sliding parcel owing to inertial compression is evaluated to be $\Delta\zeta_z = 0.5 \times 10^{-5}\,s^{-1}$. This is too weak to account for the rapid development of the systems considered here. Thus, SVD must be the main mechanism for the formation of the SW vortex.

6. Slantwise vorticity development in a saturated atmosphere

Based on the Boussinesq approximation and using the wet-bulb potential temperature, Bennetts and Hoskins (1979) studied the properties of moist potential vorticity, and obtained an equation to describe its variation. The subject was also investigated by Wu et al. (1995) based on the accurate primitive equation system. They found that, for a saturated atmosphere which is adiabatic and frictionless, its moist potential vorticity (MPV) is conserved:

$$\frac{DP_m}{Dt} = 0 \tag{23}$$

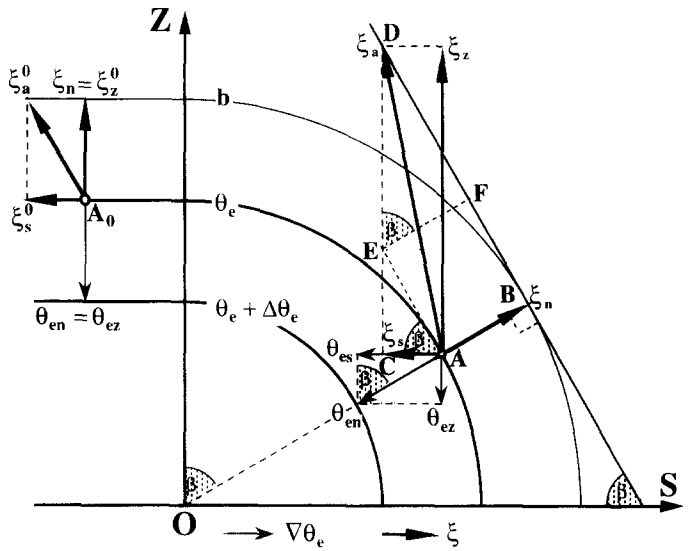

Fig. 6. Schematic diagram showing the development of vertical vorticity in a saturated atmosphere owing to the slantwise sloping of moist isentropic surfaces. When a parcel A_0 is initially on the horizontal part of a θ_e surface, MPV = $\xi_n^0\theta_{en}$ is independent of ξ_s. When it slides down the θ_e surface at an angle $\beta(>0)$ to A, $\xi_z = (\xi_n/\cos\beta) - \xi_s\tan\beta$. Now, the increase in $|\xi_s|$ or in β may result in the development of ξ_z.

or the MPV:

$$P_m = \alpha\boldsymbol{\zeta}_a \cdot \nabla\theta_e = \text{constant} \tag{24}$$

where the equivalent potential temperature

$$\theta_e = \theta\exp(Lq/C_pT_b) \tag{25}$$

and T_b is the pseudo wet-bulb temperature. It is obvious that the 'box law' and the 'circumscribed plane law' in the case of dry atmosphere is still applicable in the case of saturated atmosphere except that now θ_e rather than θ should be used.

To extend the theory of down-sliding SVD from dry atmosphere to moist atmosphere, we need to assume that (1) the atmosphere is saturated, and (2) the speed of down-sliding of a parcel at a θ_e surface is slow enough so that the properties of the parcel are well mixed with those of the environment.Following a similar procedure, we can obtain a formula much like Eq. (8):

$$\xi_z = (\xi_n\theta_{en} - \xi_s\theta_{es})/\theta_{ez}, \quad (\theta_{ez} \neq 0) \tag{26}$$

Similarly, we assume, in Fig. 6, that the parallel moist isentropes θ_e are horizontal to the left of the z-coordinate, but are bent as circles to its right, and that the gradient of θ_e is constant. In the same way we define the down-slope angle β. In Fig. 6, down-sliding corresponds to increasing β, whereas in Fig. 2 down-sliding corresponds to decreasing β. This is because Fig. 2 was designed for a dry atmosphere, and Fig. 6 for a saturated atmosphere. Imagining that the horizontal coordinate s is pointing northward, then Fig. 2 looks like the distribution of isentropes along a mid-latitude cold front which is

usually statically stable. On the other hand, Fig. 6 looks like the distribution of moist isentropes in front of a northward moving subtropical warm and moist tongue as shown in Fig. 9 (below). According to Fig. 6,

$$\tan\beta = \theta_{es}/\theta_{ez}, \quad (-\pi/2 < \beta < \pi/2) \tag{27}$$

so that

$$\cos\beta = \theta_{ez}/\theta_{en} > 0$$

Substituting these into Eq. (26) leads to Eq. (10) as well. Assuming that the condition

$$C_M = \xi_s\theta_{es}/\theta_{ez} < 0 \tag{28}$$

is satisfied, then we obtain the same expression for ξ_z as Eq. (12), which is an increasing function of $|\beta|$, and can be interpreted by using Fig. 6. As the air parcel is sliding down the θ_e surface, β is increasing, and ξ_z is also increased.

Following a procedure similar to deducing Eq. (14) and Eq. (15), the vertical vorticity tendency equation for a saturated atmosphere can be obtained as

$$\frac{D\zeta_z}{Dt} + \beta v + (f+\zeta_z)\nabla\cdot V = -\frac{1}{\alpha(\theta_{ez})^2}\left[(P_m - \xi_s\theta_{es})\frac{D\theta_{ez}}{Dt} + \theta_{ez}\xi_s\frac{D\theta_{es}}{Dt} + \theta_{ez}\theta_{es}\frac{D\xi_s}{Dt}\right], \quad \theta_{ez}\neq 0 \tag{29}$$

or,

$$\frac{1}{\alpha}\frac{D\xi_z}{Dt} = \frac{D\zeta_z}{Dt} + \beta v + (f+\zeta_z)\nabla\cdot V = \frac{1}{\alpha}\frac{D}{Dt}\left[\frac{P_m}{\theta_{ez}} - C_M\right], \quad \theta_{ez}\neq 0 \tag{30}$$

Eq. (29) describes how the changes in convective stability θ_{ez}, moist baroclinity θ_{es}, and vertical wind shear ξ_s affect the development of vertical vorticity. According to Eq. (30), the SVD condition for ζ_z or ξ_z in saturated atmosphere becomes

$$C_M(t+\Delta t) - C_M(t) < P_m\left[\frac{1}{\theta_{ez}(t+\Delta t)} - \frac{1}{\theta_{ez}(t)}\right], \quad \theta_{ez}\neq 0 \tag{31}$$

or

$$C_M(\beta+\Delta\beta) - C_M(\beta) < P_m\left[\frac{1}{\theta_{ez}(\beta+\Delta\beta)} - \frac{1}{\theta_{ez}(\beta)}\right], \quad \theta_{ez}\neq 0 \tag{32}$$

According to these, no matter how the slantwise isentropes are located and what signs of the initial values of ζ_z, ξ_z and P_m are, SVD will occur so long as the condition Eq. (31) or Eq. (32) is satisfied. Again, it can be seen that condition Eq. (28) is a sufficient condition for SVD.

7. Formation of low-level jet (LLJ) in a convectively unstable atmosphere

Let us consider the impact on vertical wind shear of a parcel which is sliding down a θ_e surface as shown in Fig. 6 and Fig. 7 from A_0 to approach ground surface and

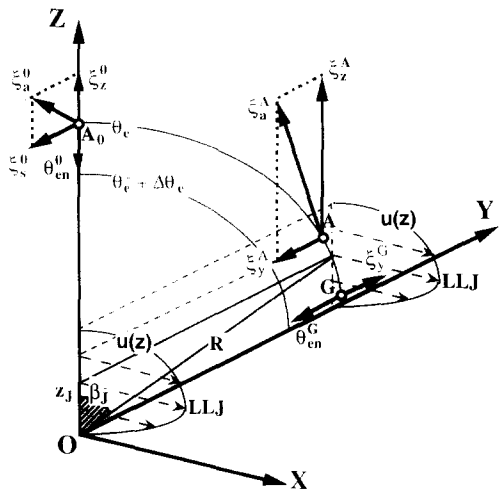

Fig. 7. Schematic diagram showing the relationship between slantwise vorticity development and low-level jet (LLJ). In a convectively unstable atmosphere under the constraint of the conservation of moist potential vorticity, slantwise vorticity development should be accompanied by the development of a low-level jet.

experiencing slantwise vorticity development. We concentrate our attention on a convectively unstable atmosphere. For simplicity, we also assume the horizontal coordinate S in Fig. 6 to be northward as shown in Fig. 7. Because in this case $\theta_{es} < 0$, and as the atmosphere is convectively unstable, the condition Eq. (28) implies that SVD will occur at the levels (e.g. A) where westerlies decrease with increasing height;

$$(\xi_s)_A = (\xi_y)_A = \left(\frac{\partial u}{\partial z}\right)_A < 0$$

Further, we consider the near-boundary condition at an elevation G which is close to but not at the 'ground surface'. Because when β approaches $\pi/2$, θ_{ez} approaches zero, and because, from Eq. (26) and Fig. 7, $(\mathrm{MPV})_{A_0} = \xi_z \theta_{en}$ at A_0, and $(\mathrm{MPV})_G \approx \xi_s \theta_{es} \approx \xi_s \theta_{en}$ at G, the conservation of MPV requires

$$(\xi_s \theta_{en})_G \approx (\xi_z \theta_{en})_{A_0}, \text{ when } \beta \to \pi/2$$

Because $(\theta_{en})_G = (\theta_{en})_{A_0}$ as was assumed, we then have

$$(\xi_s)_G \approx (\xi_z)_{A_0} > 0, \text{ when } \beta \to \pi/2 \tag{33}$$

For our case, Eq. (33) implies that when the down-sliding parcel approaches the ground surface, the vertical wind shear ξ_s should change its sign. In the case shown in Fig. 7, westerlies near the surface should increase with height,

$$(\xi_s)_G = (\xi_y)_G = \left(\frac{\partial u}{\partial z}\right)_G > 0$$

When massive flow experiences the same procedure, the above discussions lead us to the conclusion that a jet-like maximum wind speed should be formed at a low level

$z = z_J$ above the surface and below level A (Fig. 7). We let R be the radius of curvature of the θ_e surface, and β_J, the slantwise angle at the LLJ level. Because, at z_J, where the wind speed is maximum, $\xi_s (= \partial u/\partial z)$ vanishes, then from Eq. (26) the vertical vorticity at z_J is

$$\xi_z^J = \xi_n \theta_{en}^J / \theta_{ez}^J = \xi_n / \cos \beta_J = \xi_n R / z_J, \quad \theta_{ez}^J \neq 0 \tag{34}$$

This implies that the intensity of the vertical vorticity at the LLJ level is inversely proportional to the geometric height z_J of the LLJ. The lower the LLJ, the stronger the vertical vorticity. In addition, because ξ_s changes its sign below z_J, the condition Eq. (28) will be violated and SVD stops. Then the vertical vorticity at z_J should be the maximum for the parcel during its down-sliding.

8. MPV analysis of a torrential rain process

For convenient application of the SVD theory to routine analysis, here we adopt the p-coordinate once more, and define the vertical and horizontal components of MPV as, respectively,

$$\begin{cases} \text{MPV1} = \xi_p \theta_{ep} = -g \zeta_p \dfrac{\partial \theta_e}{\partial p}, \\ \text{MPV2} = \xi_s \theta_{es} = -g \boldsymbol{k} \times \dfrac{\partial \boldsymbol{V}}{\partial p} \cdot \nabla_p \theta_e \end{cases} \tag{35}$$

then

$$P_m = \text{MPV} = \text{MPV1} + \text{MPV2} = \text{constant} \tag{36}$$

The condition Eq. (28) for SVD can be expressed as

$$C_M^p = \text{MPV2}/\theta_{ep} > 0 \tag{37}$$

This means that when SVD occurs, the horizontal component of MPV and the convective stability possess the opposite signs. It can be readily shown that with the geostrophic relation

$$\text{MPV2} = -\frac{\alpha g}{f \theta_0} \nabla_p \theta \cdot \nabla_p \theta_e < 0 \tag{38}$$

Therefore, an atmosphere which is geostrophic (MPV2 < 0) and convectively stable ($\theta_{ep} < 0$), or strongly ageostrophic (MPV2 > 0) and convectively unstable ($\theta_{ep} > 0$), satisfies the condition Eq. (37) for SVD.

The occurrence and development of torrential rain are usually associated with the rapid developments of convergence of low-layer flow and rising motion, accompanied by dramatic growth of vertical cyclonic vorticity. The mechanism of development of cyclonic vorticity is therefore one of the important issues in the study of torrential rain occurrence (Tao, 1980). In the above sections we have shown how cyclonic vorticity can develop dramatically when air parcels down-slide on very steep θ_e surfaces, and how the

horizontal moist potential vorticity MPV2 is associated with this down-sliding SVD. In the rest of this section we try to use this SVD theory to analyse the occurrence of torrential rain along a monsoonal front.

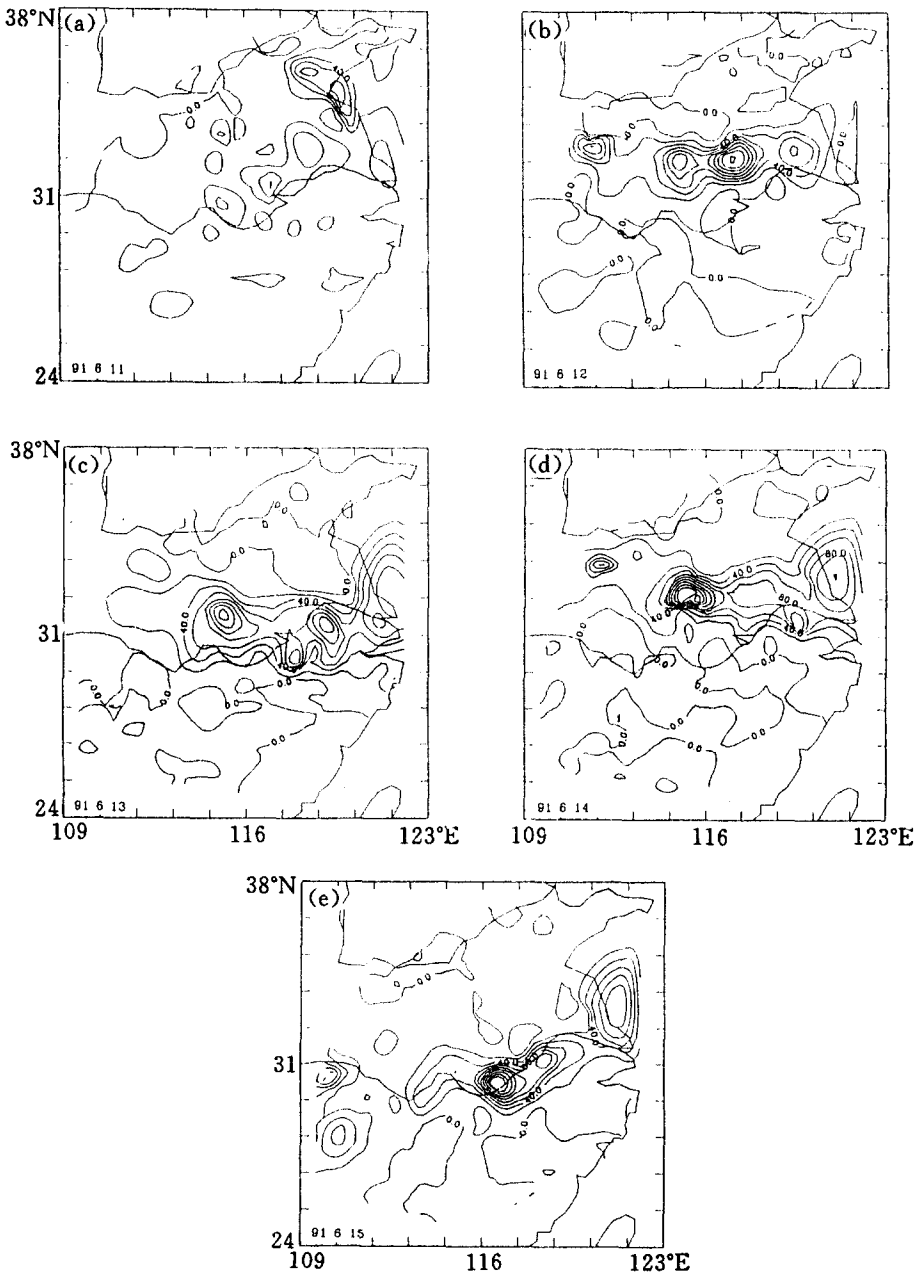

Fig. 8. Distribution of 24h precipitation from 11 to 15 June 1991. Contour interval in 20mm.

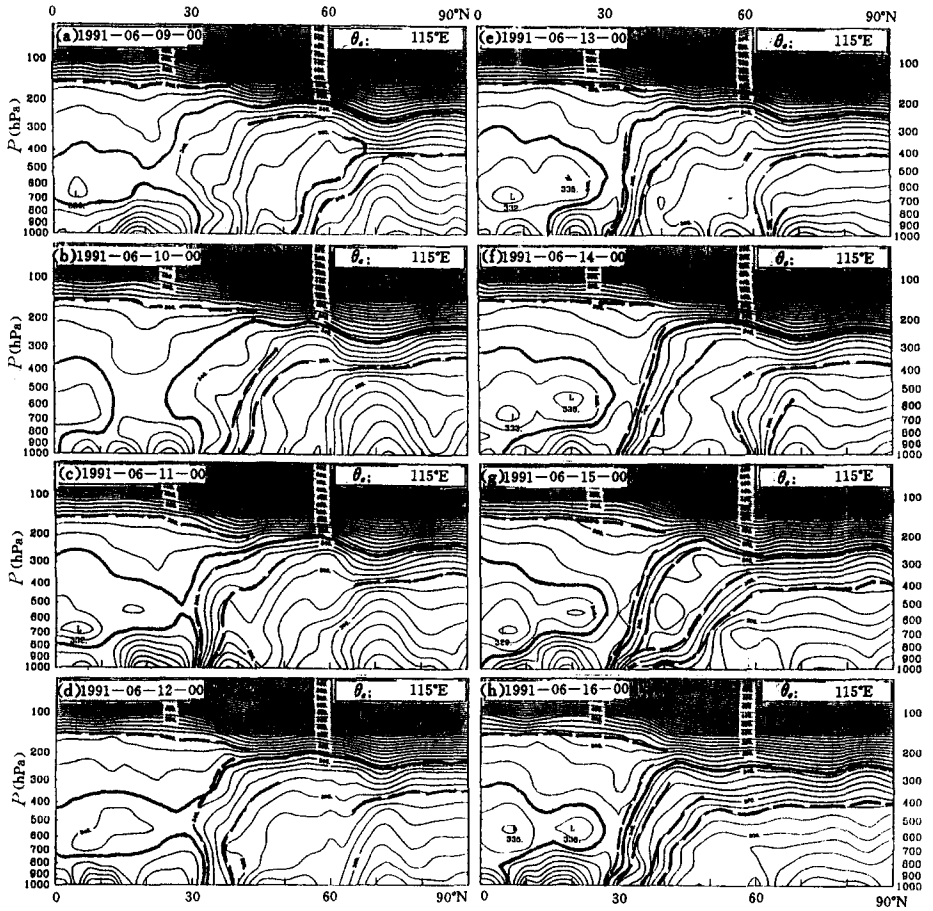

Fig. 9. Distribution of θ_e in the cross-section along 115°E at 00:00h from 9 to 16 June 1991. Bold curves indicate moist isentropic $\theta_e = 345$ K, bold dashed curves mark the locations of the θ_e front and tropopause.

In June 1991 over East Asia, the subtropical high over the northwestern Pacific was abnormally strong. The trough over the Bay of Bengal was also stronger than normal, and located to the east of its climate mean position. In middle latitudes, there were frequent synoptic-scale systems propagating eastwards. In the middle of the month, cold air came from Northwestern China, and intercepted low layer southwesterlies from the Bay of Bengal in the middle and lower reaches of the Yangtze and Huai River. Persistent torrential rain was observed in the region from 11 to 15 June (Dong, 1991). As shown in Fig. 8, from 12 to 15 June and along the latitude zone between 30°N and 33°N the centres of torrential rain all exceeded or were close to 150 mm day^{-1}, and serious flooding occurred. Fig. 9 shows the north–south cross-sections of θ_e along 115°E at 00:00h from 9 to 16 June 1991. This longitude is chosen because it is typical of where the persistent rainfall occurred. Initially, warm and moist and convectively

unstable ($\theta_{ep} > 0$) air was located to the south of 31°N. The cold and dry air from high latitudes was characterised by a front with a band of concentrated θ_e surfaces. This gradually moved southward from 50°N. On 11 June, this θ_e front invaded the moist,

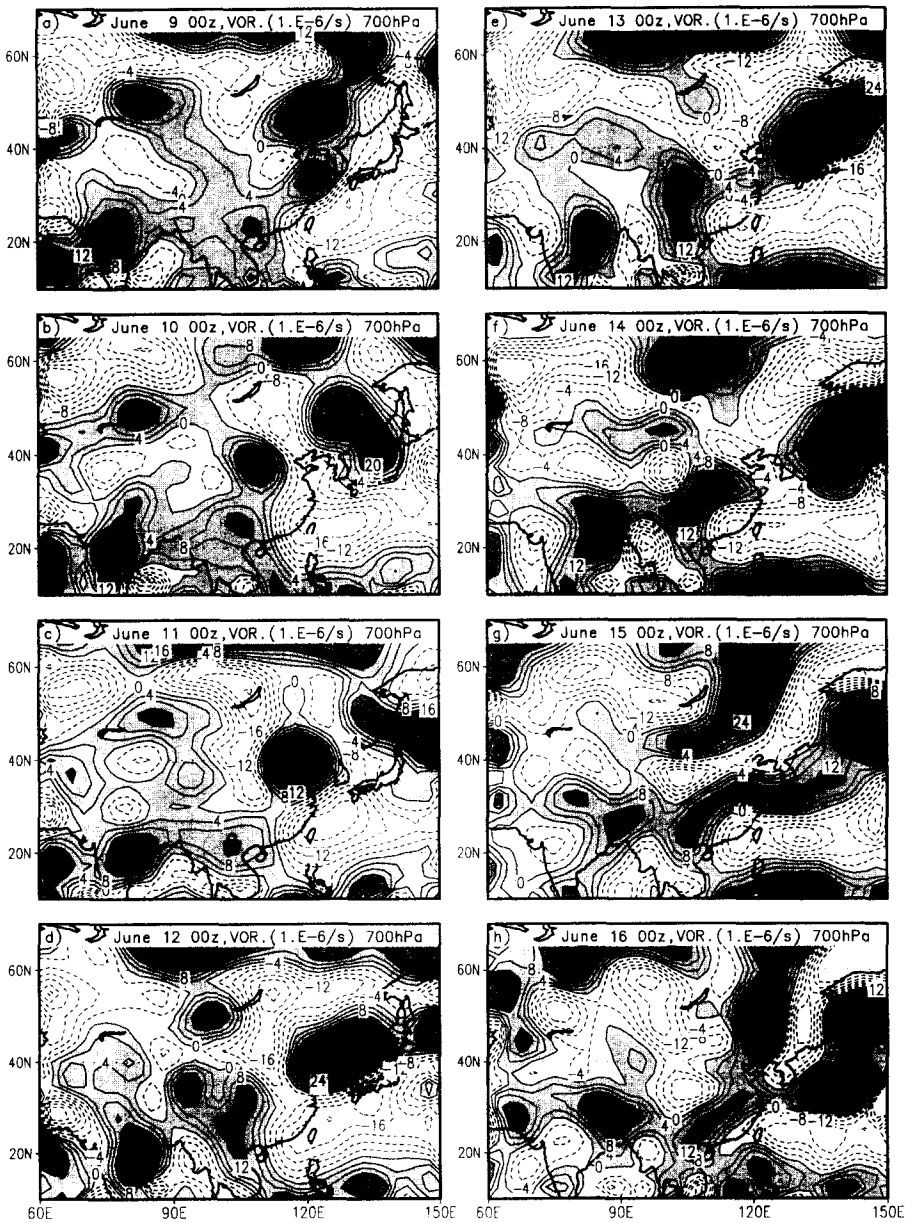

Fig. 10. Evolution of the vertical vorticity ζ at 700hPa and 00:00h from 9 to 16 June 1991. Interval is $0.4\times10^{-5}\,s^{-1}$. Dashed curve indicates negative value, and shading indicates positive values. Heavy shading denotes where ζ is greater than $1.2\times10^{-5}\,s^{-1}$.

convectively unstable, region in the south, and torrential rain started to occur in the sector of steep and dense θ_e band. Then, cold and warm air converged and torrential rain continued. On 14 June, another subpolar front formed in high latitudes and moved southward. On 15 June, this fresh cold air merged into the monsoon front, warm and moist air retreated to the south of 29°N, and the persistent rainfall then ended. Carefully analysing Fig. 8, one finds that, every day, torrential rain occurred where the θ_e surfaces aloft are very steep, in favour of slantwise vorticity development.

In Fig. 10 is shown the evolution of vertical vorticity at 700 hPa and 00:00 h from 11 to 16 June 1991. On 10 June, there was a mid-latitude high vorticity centre denoted by α which moved eastwards. On 11 June, this centre reached Bohai Bay and caused severe rainfall appearing to its south. At the same time, there was another weak centre (denoted by β) at 20°N, with an intensity of $1.2 \times 10^{-5}\,s^{-1}$. From 11 to 15 June, as this system moved slowly northeastward towards the Yangtze River Reaches, its intensity grew rapidly to $2.0 \times 10^{-5}\,s^{-1}$, and the area with more than $1.2 \times 10^{-5}\,s^{-1}$ expanded greatly, in accordance with the development of torrential rain shown in Fig. 8. On 14 June, accompanying the development of the subpolar front, there appeared high vorticity centres near Lake Baikal. As this mid-latitude system moved southeastward, on 15 June the high vorticity centre along the Yangtze River Reaches was weakened. Its main centre had moved to the western Pacific. On 16 June, the mid-latitude system had swept over Northern China, and the remained part of the southern centre had retreated to Southern China. Torrential rain along the Yangtze River thus stopped.

The evolution of the 850 hPa wind during the same period is shown in Fig. 11. Southerlies existed over Southern China before 15 June. As the tropical high vorticity centre at 20°N developed on 11 June (Fig. 10(c)), the wind direction in front of the centre changed to northeastward, forming a southwesterly jet with an intensity of more than $15\,m\,s^{-1}$. This LLJ persisted till 15 June. In comparison with the distribution of θ_e as shown in Fig. 9, the motion of the down-sliding θ_e surface of southerlies can be identified in the area north of about 25°N. It is notable that during the periods from 10 to 12 June and from 13 to 15 June, the westerly component of the LLJ was intensified. As we will show in the following discussion, SVD did exist in the torrential area before 15 June. Therefore the intensification of the westerly component of the LLJ could be well interpreted by the theory developed in Section 7 and Fig. 7. On 16 June, as the northerly swept over eastern China, SVD stopped, and the LLJ disappeared from southern China.

Fig. 12 shows the evolution of MPV1 at 700 hPa in the same period. It can be seen that its distribution in the lower troposphere corresponds well to that in upper layers (figures not shown). For example, a high MPV1 system which was in Northwestern China on 9 June travelled regularly southeastwards. From 11 June, the high MPV1 air over Northern China which was convectively stable confronted, along the Jiang-Huai Reaches, the convectively unstable atmosphere over Southern China. Persistent torrential rain then started to occur near the edge of the convectively unstable region in front of the high MPV1 system. On 16 June, as the convectively stable air occupied the region south to the Yangtze River, torrential rain stopped.

In Fig. 13 is shown the evolution of horizontal component MPV2 at 700 hPa in the same period. It is remarkable that during this period along the Yangtze River, there existed an elongated band of positive MPV2. This is because in this period at 700 hPa,

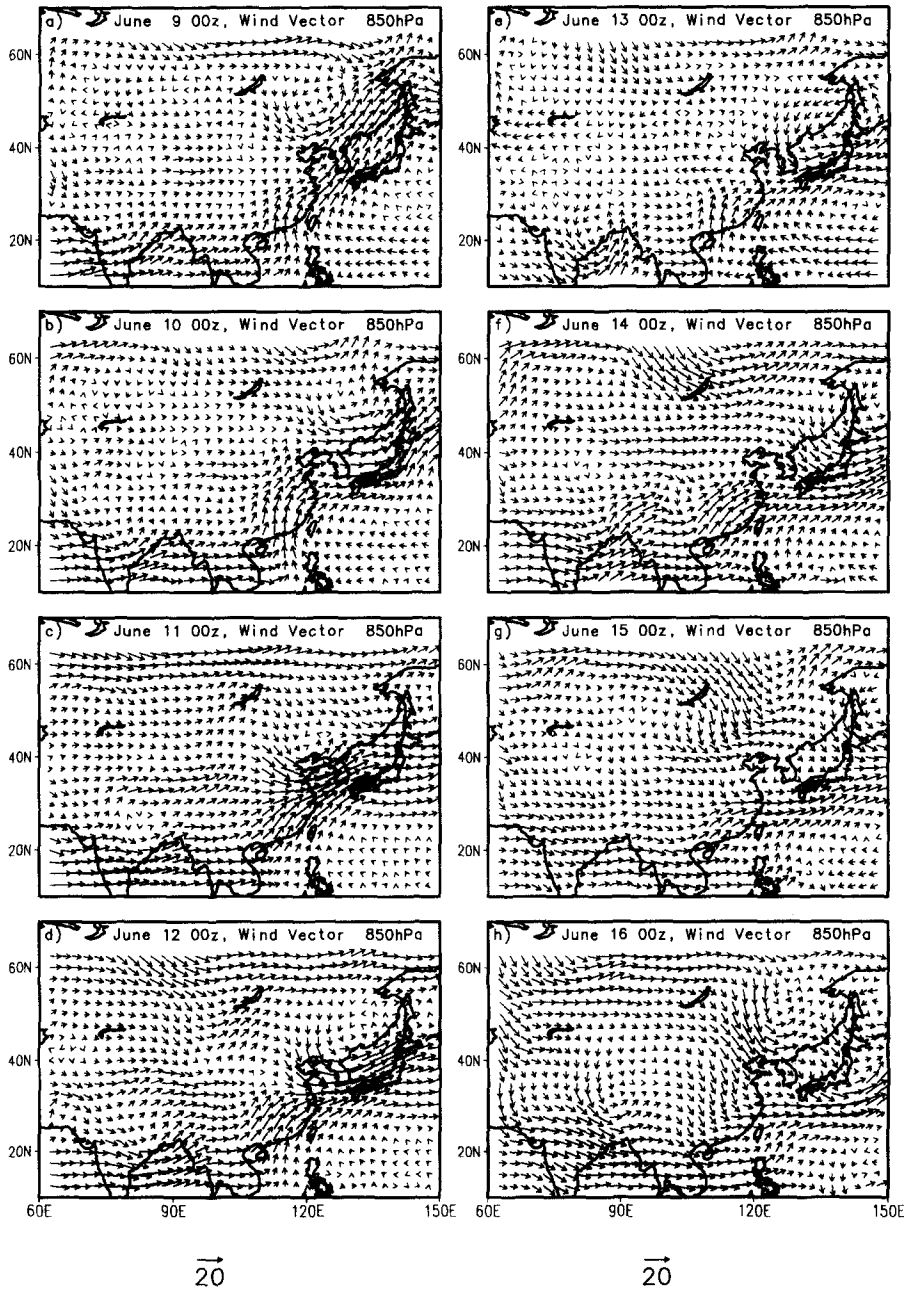

Fig. 11. Evolution of the wind vector at 700 hPa and at 00:00 h from 9 to 16 June 1991. The scaling of the wind vector is shown at the bottom of the figure (in $m\,s^{-1}$).

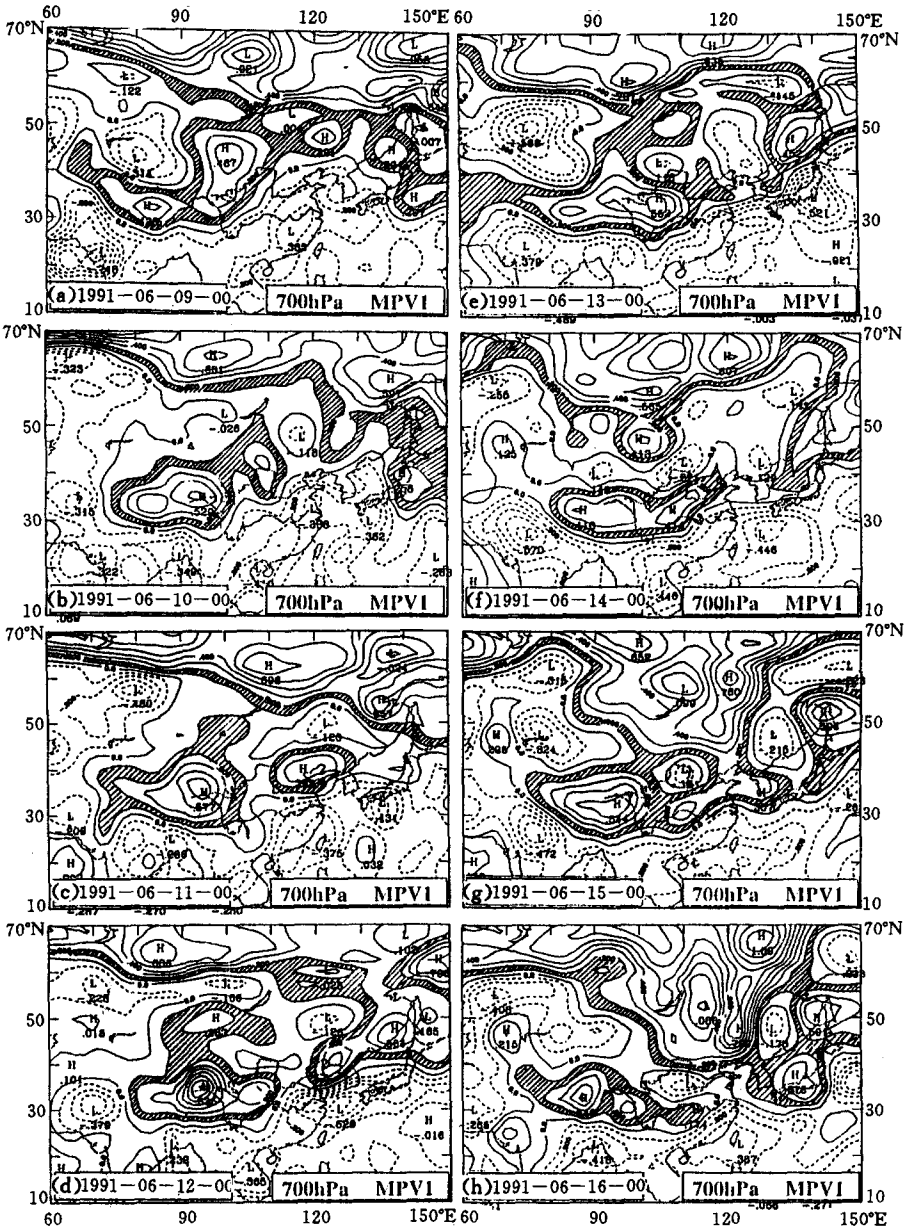

Fig. 12. Evolution of the vertical component MPV1 of moist potential vorticity at 700 hPa and at 00:00 h from 9 to 16 June 1991. Dashed curves denote negative values. Contour interval in 0.1 PVU. The area between 0.1 and 0.2 PVU is hatched.

the warm and moist air was to the south of the Yangtze River, and the LLJ existed below 700 hPa (Dong (1991); also refer to Fig. 11). Thus along the Yangtze River, $\partial u/\partial z < 0$, $\partial \theta_e/\partial y < 0$, and MPV2 became positive. The appearance of positive MPV2

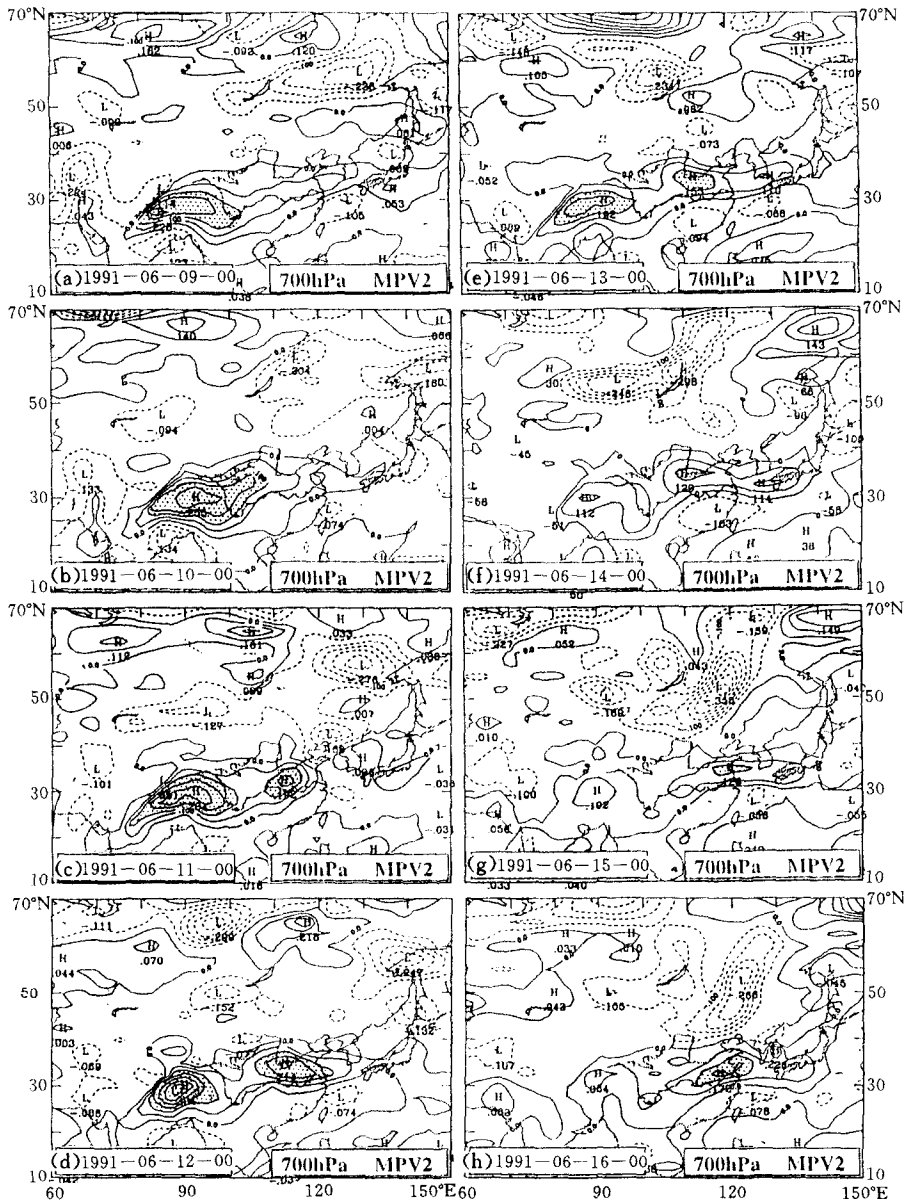

Fig. 13. Evolution of the horizontal component MPV2 of moist potential vorticity at 700 hPa and at 00:00 h from 9 to 16 June 1991. Dashed curves denote negative values. Contour interval in 0.05 PVU. Dotted area presents high positive region with MPV2 > 0.1 PVU.

in the Jiang-Huai region during the period of monsoonal torrential rain thus revealed that in this area, there was no geostrophic balance between wind and pressure fields. According to Fig. 6 and Fig. 7, the increase in the intensity of LLJ or of warm and moist

air advection will increase the positive MPV2. Therefore the movement of positive MPV2 in the lower troposphere can serve as a tracer of the activities of LLJ and warm and moist current. As seen in Fig. 13, a high positive MPV2 centre was located on the southeastern flank of the Tibetan Plateau on 9 June. Later, it stretched eastward along the Yangtze River. On 11 June, a new positive MPV2 centre, which was separated from the main centre, moved eastward and reached the convectively unstable (MPV1 < 0; see Fig. 12) region in Jiang-Huai Reaches. According to Eq. (37), the condition for SVD $C_{\mathrm{M}}^{p} > 0$ is satisfied, and ξ_z will also increase, in favour of low-level convergence and ascent, torrential rain starting to appear where the θ_{e} surfaces are almost vertical. Afterwards, this high MPV2 centre remained in the region and torrential rain persisted. In the mean time, the high MPV2 centre to the southeast of the Tibetan Plateau decayed locally, indicating the weakening of the warm and moist southwesterly current. On 16 June, as the convectively unstable region at 700 hPa retreated from the Yangtze River Reaches (Fig. 7), and with the departure of the already weakened positive MPV2 centre from the continent to the Pacific, the persistent torrential rain then ended.

It is interesting to note that for an inertially stable atmosphere ($\xi_z > 0$), condition Eq. (37), i.e. $C_{\mathrm{M}}^{p} > 0$, together with MPV2 > 0 are at least in our case equivalent to the condition for moist symmetric instability (MPV < 0). This is because when C_{M}^{p} and MPV2 are both positive, MPV1 $= \xi_p \theta_{\mathrm{e}p} < 0$. From Fig. 12 and Fig. 13, we see that in the heavy rain region $|\mathrm{MPV1}| > |\mathrm{MPV2}|$. Then the sign of MPV is determined by that of MPV1. Therefore, our result is in agreement with the contentions of Bennetts and Hoskins (1979) and Emanuel (1984) that moist symmetric instability is the cause of some heavy rainbands.

9. Discussion and conclusions

Based upon the conservation of Ertel potential vorticity and MPV, the theory of slantwise vorticity development was discussed in this study. It was found that if θ or θ_{e} surfaces are steep, when air slides down at such surfaces, cyclonic vorticity is easy to develop dramatically. Compared with the development theory based on moist isentropic coordinates, the theory of slantwise vorticity development associated with moist baroclinity based on z-coordinate or p-coordinate possesses some remarkable advantages. θ_{e} surfaces near a monsoonal front are usually sloping. ζ_θ in θ_{e} coordinate which is perpendicular to θ_{e} surface then is not perpendicular to the Earth's surface. Thus, the change in ζ_θ is not equivalent to the change in vertical vorticity. When z-coordinate or p-coordinate is used, the summation of the horizontal and vertical components of P_{m} is conserved. Now the change in $\zeta_z (\zeta_p)$ is determined either by the changes in static–convective stability, vertical wind shear or by (moist) baroclinity. Therefore, not only the decrease in static–convective stability, but also the increase in vertical wind shear or (moist) baroclinity can result in the development of vertical cyclonic vorticity. According to Eq. (14) (or Eq. (29)), the general tendency of vertical vorticity depends on the complex combination of the variations of these three parameters. The present study shows that their variations are not independent of each other, but are subject to the

constraint of conservation of (moist) potential vorticity. Thus, Eq. (14) (or Eq. (29)) can be replaced by the equivalent equation Eq. (15) (or Eq. (30)). It was shown that SVD will occur so long as the condition Eq. (11) (or Eq. (28), or Eq. (37)) is satisfied. Results from this study show that geostrophic approximation is inadequate for the analysis of torrential rain of convectively unstable type associated with a monsoonal front.

In summer, warm and moist southerlies are very active. When they meet with cold and dry northerlies, the θ_e surface in front of these southerlies is very steep, slantwise vorticity development there becomes vigorous, and torrential rain can develop dramatically. Therefore such lower tropospheric vorticity development can be an important mechanism for the formation of torrential rain.

Another important point revealed by this study is that, in a saturated atmosphere, a parcel sliding down a slantwise θ_e surface and experiencing SVD has to change the sign of its horizontal vorticity; also, the existence of a low-level jet favours SVD. The lower the jet stream, the stronger the SVD. Below the level of the LLJ, SVD ceases to occur. It seems plausible that massive down-sliding flow at a slantwise θ_e surface which is subject to SVD may induce a low-level jet. However, how the existing LLJ interacts with SVD is still not clear, as, in reality, LLJs are often observed in association with the occurrence of torrential rain and meso-scale convective systems. These questions deserve further investigation.

Finally, it is noteworthy that the theory of slantwise vorticity development is not the same as the theory of vorticity development associated with vorticity conversion from its horizontal to vertical component owing to the uneven lifting of a vortex. In the latter case, an increase in vertical vorticity requires a decrease in horizontal vorticity. The theory developed here is based upon the conservation characteristics of (moist) potential vorticity. It requires declination of (moist) isentropic surfaces. According to this theory, the development of vertical vorticity may be accompanied by the concurrent development of horizontal vorticity or moist baroclinity, and is much stronger than that due to uneven vortex lifting. The concurrent development of vertical wind shear, moist baroclinity and vertical vorticity is observed commonly in the occurrence of torrential rain associated with monsoonal front or other frontogenesis (Tao, 1980). Therefore, the process of vorticity development associated with moist baroclinity is more general in monsoon dynamics.

Acknowledgements

This study was supported by the Key Programme 'On the mechanism of the variation of high pressure systems in the subtropics' (Number 49635170) and the Programme 'Air–sea interaction over Indian Ocean and North Pacific Ocean and ENSO' (Number 49575265) of the Chinese Natural Sciences Foundation. Liqing Dong of the Chinese National Meteorological Centre provided the basic material for this study. The authors would like to thank Dr. Yongsheng Zhang and Ms. Yaping Cai for plotting part of the figures, and Ms. Yanbin Sun and Ms. Xuan Wang for typing the draft.

References

Anthes, R.A. and Heagerson, P.L., 1984. A comparative numerical simulation of the Sichuan flooding catastrophe (11–15 July, 1981). Proc. 1st Sino-American Workshop on Mountain Meteorology, Chinese Academy of Sciences and US National Academy of Sciences, Beijing. American Meteorological Society, Boston, MA, pp. 519–524.

Bennetts, D.A. and Hoskins, B.J., 1979. Conditional symmetric instability—a possible explanation for frontal rainbands. Q. J. R. Meteorol. Soc., 105: 945–962.

Bleck, R., 1984. An isentropic coordinate model suitable for lee cyclogenesis simulation. Riv. Meteorol. Aeronaut., 43: 189–194.

Chen, S.-J. and Dell'Osso, L., 1984. Numerical prediction of the heavy rainfall vortex over the eastern Asia monsoon region. J. Meteorol. Soc. Jpn., 62: 730–747.

Dong L., 1991. Persistent torrential rain in Yangtze–Huai River Reaches, and abnormal temperature in most part of China. Meteorology, 17(9): 58–61.

Emanuel, K.A., 1984. The Lagrangian parcel dynamics of moist symmetric instability. J. Atmos. Sci., 40: 2368–2377.

Ertel, H., 1942. Ein neuer hydrodynamischer Wirbdsatz. Meteorol. Z., Braunschweig S., 59: 277–281.

Hoskins, B.J., McIntyre, M.E. and Robertson, A.W., 1985. On the use and significance of isentropic potential vorticity maps. Q. J. R. Meteorol. Soc., 111: 877–946.

Hovermale, J.B., 1984. Numerical experiments with the Sichuan flooding catastrophe (11–15 July, 1981). Proc. 1st Sino-American Workshop on Mountain Meteorology, Chinese Academy of Sciences and US National Academy of Sciences, Beijing. American Meteorological Society, Boston, MA, pp. 243–264.

Kuo, Y.-H., Cheng, L. and Anthes, R.A., 1986. Mesoscale analysis of Sichuan flood catastrophe, 11–15 July, 1981. Mon. Weather Rev., 114: 1984–2003.

Tao, S., 1980. Torrential Rain in China (in Chinese). Science Press, Beijing, 225 pp.

Wu, G.-X. and Chen, S.-J., 1985. The effect of mechanical forcing on the formation of a mesoscale vortex. Q. J. R. Meteorol. Soc., 111: 1049–1070.

Wu, G., Cai, Y. and Tang, X., 1995. Moist potential vorticity and slantwise vorticity development (in Chinese). Acta Meteorol. Sin., 53(4): 387–405.

Zhao, Y.-C., Wu, G.-X., Ji, L.-R. and Liu, H., 1995. Isentropic potential vorticity diagnosis and numerical modelling of a southwest vortex by using an isentropic model (in Chinese). In: On the New Techniques in Numerical Forecast of Typhoon and Torrential Rain. Chinese Meteorogical Press, Beijing, pp. 94–102.

Zhou, X.-P. and Hu, X.-F., 1984. A brief analysis and numerical simulation of the Sichuan extraordinarily heavy rainfall event. Proc. 1st Sino-American Workshop on Mountain Meteorology, Chinese Academy of Sciences and US National Academy of Sciences, Beijing. American Meteorological Society, Boston, MA, pp. 555–565.